Space charge effects in field emission: Three dimensional theory

Kevin L. Jensen[a)]
Code 6843, ESTD, Naval Research Laboratory, Washington, DC 20375-5347, USA

(Received 15 June 2009; accepted 10 November 2009; published online 5 January 2010)

Field emitters rely on high gradients on microfabricated structures to enable substantial levels of emitted current, which can in turn act to reduce the field at the emission site of a single emitter. An account of that effect is obtained in the following steps: a model of the emitter geometry based on the point charge model that allows for the determination of the apex radius and field enhancement factor for arbitrarily sharp emitter structures is given, followed by an analytical formula for the calculation of total current from such a structure and then by a model of the effect of emitted current in suppressing the field at the emission site. Predictions of the impact of space charge on the emitted current are made and compared to findings of Barbour *et al.* [Phys. Rev. **92**, 45 (1953)] for sharpened structures with varying work function. A discussion is given of the method to combine single tip three-dimensional results with a study of space charge on field emission in one dimension. [doi:10.1063/1.3272688]

INTRODUCTION

Field emitters are high brightness electron sources under investigation for a variety of applications, such as electron beam lithography[1,2] and transmission electron microscopes,[3] spacecraft propulsion,[4,5] millimeter-wave vacuum electronic amplifiers and terahertz devices,[6–8] and advanced particle accelerators and free electron lasers (FELs).[9–13] Their operation can be affected by the fields from the charges they emit if those fields reduce the extraction field at the emission sites, and such consequences are termed "space charge effects." Such effects can induce undesirable growth in the dimensions of the beam as it propagates, as commonly accounted for in the beam envelope equation;[14] a related metric of beam quality in that equation is called "emittance" and refers to the tendency of a beam to spread as it propagates due to transverse velocity components in the electron distribution function. An account of both space charge and emittance from field emitters is required to model how the beam changes as it propagates. In the present study, an examination is undertaken of the space charge forces that can exist in the vicinity of a single emitter; separate studies consider space charge effects associated with an array of emitters[15] and estimations of the emittance of a single tip and an array.[16]

In vacuum electronic devices, particle accelerators, and free electron lasers,[6–8] electron sources are often run space charge limited (in the case of thermal sources) or at such high current densities (in the case of photocathodes in rf injectors[17–19]) that an understanding of space charge and emittance growth at the cathode is essential. As increasingly brighter beams, shorter bunches, and/or emission modulation are sought, field emitter arrays have been under consideration. The simulation of intense sources is the domain of highly capable particle-in-cell (PIC) simulation codes[20–23] which do have field emission algorithms[24] but in the case of field emission from realistic sources, accounting for space charge is hampered by the many orders of magnitude disparity between the dimensions of the emitting structures and the beam acceleration and transport region [not to mention the inherently three dimensional (3D) nature of an array of field emitters is in contrast to the usual two dimensional (2D) rotational symmetry of the electron beam]. While in principle, meshing a grid to the dimensions of the emitter site is possible, the current density, grid and macroparticle size, and time step (if non-static) are inter-related such that computational overhead demands make fine grids a burden, and so a one dimensional (1D) Fowler–Nordheim (FN) equation utilized over the area of the cathode with a factor relating surface field to anode voltage is often employed. Even though the promise of high brightness electron sources such as field emitters generates a strong incentive to model them in beam codes, the magnitude of the current density at the emission site indicates ignoring space charge effects on emission and emittance for operational performance levels is ill advised.

A coherent theory of field emission topical to vacuum electronics, accelerators, and free electron lasers in particular requires, first, an account of space charge and emittance for such sources under macroscopic and possibly low dimensional environments, second, an account of the microscopic and fully 3D regions near the emitter site, and, third, a characterization of the beam that is to be produced (emittance). The present work addresses the second requirement, as the first and third are the subject of separate studies,[15,16] although a consideration of the methods to hand off electron distributions from the microregime (the unit cell or single emitter region) to the macroregime (the anode-cathode or beam transport region) is common to all.

Therefore, here, a methodology for the analysis of space charge forces on the emission process within the unit cell is described, and a manner in which 1D methods may be brought to bear on arrays of emitters operating together is presented. Apart from providing a comprehensive theoretical account, the approach presented is intended to provide a framework to investigate field emitters without intensive numerical efforts in a manner amenable to PIC codes for when

[a)]Electronic mail: kevin.jensen@nrl.navy.mil.

Report Documentation Page

Form Approved
OMB No. 0704-0188

1. REPORT DATE	2. REPORT TYPE	3. DATES COVERED
JUN 2009		**00-00-2009 to 00-00-2009**

4. TITLE AND SUBTITLE	5a. CONTRACT NUMBER
Space charge effects in field emission: Three dimensional theory	5b. GRANT NUMBER
	5c. PROGRAM ELEMENT NUMBER
6. AUTHOR(S)	5d. PROJECT NUMBER
	5e. TASK NUMBER
	5f. WORK UNIT NUMBER
7. PERFORMING ORGANIZATION NAME(S) AND ADDRESS(ES) **Naval Research Laboratory,Code 6843, ESTD,Washington,DC,20375**	8. PERFORMING ORGANIZATION REPORT NUMBER
9. SPONSORING/MONITORING AGENCY NAME(S) AND ADDRESS(ES)	10. SPONSOR/MONITOR'S ACRONYM(S)
	11. SPONSOR/MONITOR'S REPORT NUMBER(S)

12. DISTRIBUTION/AVAILABILITY STATEMENT
Approved for public release; distribution unlimited

13. SUPPLEMENTARY NOTES

14. ABSTRACT

15. SUBJECT TERMS

16. SECURITY CLASSIFICATION OF:			17. LIMITATION OF ABSTRACT	18. NUMBER OF PAGES	19a. NAME OF RESPONSIBLE PERSON
a. REPORT **unclassified**	b. ABSTRACT **unclassified**	c. THIS PAGE **unclassified**	**Same as Report (SAR)**	**9**	

space charge is an issue and the cathode area is but a small region of the simulation. The theory unfolds as follows. First, a point charge model (PCM) is modified to treat a well-studied class of emitters otherwise known as Spindt-type field emitter arrays.[25–28] The revised PCM overcomes the disparity in length scales between the emission site and the overall dimensions of the emitter to predict apex field and field fall-off quite accurately. Next, an analytical method to calculate the total emitted current from a single tip is developed. From the total emitted current, an estimate of the impact of space charge on a single emitter is developed. The "macroscopic" field near the cathode boundary[15] functions as the "far field" in the vastly smaller unit cells under consideration in the present study. Finally, a comparison of the single emitter space charge effects is made with a study by Barbour *et al.*[29] in which changes in I(V) characteristics changed as the work function of the emitter apex was systematically altered through the application of barium.

RELATION TO THE 1D THEORY

The potential away from an array of emitters (ungated or otherwise) rapidly becomes uniform at scales larger than the tip-to-tip spacing.[15] The nature in which the field near the emitter site changes as the distance from the emitter apex becomes comparable to the tip-to-tip spacing is therefore topical. In the PCM emitters are approximated as aggregates of point charges. Presently, the discussion here needs only to consider a single point charge to advance the argument, and so the question becomes how the field varies for a single point charge as compared to an array. The constant background field F of the 1D theory is intuitively related to how the field changes as the distance from the array of emitters increases, and showing that relation proceeds as follows. In units of the tip-to-tip spacing l, the width of the array is M, the anode to cathode separation is $N/2$, and it is assumed that $N \ll M$ to approximate the 1D configuration. The anode is at $N/2$ to make the potential there explicitly nonvarying in the transverse coordinates and is accomplished by charges (essentially image charges) at N. The field between oppositely charged planes of point particles is then

$$\hat{z}\cdot\mathbf{F} = \frac{1}{4\pi}\left(\frac{\lambda}{4\pi\varepsilon_o a_0^2}\right)\sum_{j=-M}^{M}\sum_{k=-\sqrt{M^2-j^2}}^{\sqrt{M^2-j^2}}\varphi'_{j,k}(x,y,z)$$
$$= F_o\left\{1 - \frac{z}{2\sqrt{M^2+z^2}} - \frac{(N-z)}{2\sqrt{M^2+(N-z)^2}}\right\}, \quad (1)$$

where the top line is the sum over discrete point charges, the bottom line is the on-axis large M limit in which the sums are replaced by integrals, $N/2 \ll M$ is the cathode to virtual anode separation, λ is the magnitude of the individual point charges, $F_o = \lambda/4\pi\varepsilon_0 l^2$ is the infinite plane (capacitor plate) field, φ [with the coefficient of the summation in Eq. (1)] is proportional to the potential associated with an anode-cathode pair of point charges, or

$$\varphi_{i,j}(\mathbf{r}) = \frac{1}{\sqrt{(i-x)^2+(j-y)^2+z^2}} - \frac{1}{\sqrt{(i-x)^2+(j-y)^2+(N-z)^2}}, \quad (2)$$

and $\varphi'_{i,j} = \partial_z \varphi_{i,j}$ (the z component of the field is the largest component, and therefore considered by itself for ease). The remaining terms are defined in Table I. For very large M, augmenting a transverse coordinate (x or y) by l does not measurably affect the potential (for $M=\infty$, it has no effect at all), so it shall be assumed that x and y are both smaller than $1/2$ in units of l. It is expected that near the center emitter for $z<1$ (that is, within the "unit cell"), the z component of the field for the center point charge should dominate, but that for $z>1$, then the field should be significantly more insensitive to variations with z and less directly correlated with a single charge. This intuition can be shown valid by considering the case $M=2N=40$, and, in particular, the z component of the field of the point charge and the array of charges for on axis ($x=y=0$) and at the lowest point of the potential off axis ($x=y=1/2$). As shown in Fig. 1, the center point charge field fades as $1/z^2$ until at the unit cell boundary $z \approx 1$, it is overshadowed by both the on-and off-axis fields due to the array, which have asymptotically approached the analytical form shown in Eq. (1). Therefore, the unit cell is defined by the region $-1/2 < x,y \leqslant 1/2$ and $0 < z \leqslant 1$, as schematically suggested in Fig. 2. The $z=1$ boundary can be assumed to be a constant over the region of the virtual cathode which takes its place, and the virtual cathode can then serve as the boundary for the 1D studies.[15] In such a way, the considerations of space charge near the emitter (unit cell and 3D) can be separated from the anode-cathode (1D) region that is the normal realm of the simulations modeling space charge limited current.

THE 3D MODEL

A limitation of a 1D field emission model in the analysis of space charge is that generic field emitters emit over square nanometer scale sites that are spatially separated (e.g., Table III of Ref. 30) because the sites have a high degree of curvature to enable fields of GV/m from background fields of order O(100 MV/m), potential differences on the order of 10 kV for ungated geometries or 100 V for gated geometries. The impact of space charge on field emission from multidimensional geometries is difficult, not only because finding the field gradient along a curved surface over which only a small portion emits is difficult but also because available emission equations are inherently 1D by virtue of the solution of Schrödinger's equation for current density. Therefore, the emitted current is obtained by considering modifications to the parallel plane case (as done by Barbour *et al.*[29] and Lau *et al.*[31]) or by integrating the local 1D current density for a given field gradient over a multidimensional surface of the conductor.[32]

Finding solutions to the field variation over the surface of the emitter is not trivial. Exact conformal methods can be used in 2D,[33,34] as can prolate spheroidal techniques in 3D.[35–38] Numerical methods are available[39–41] with effort.

TABLE I. List of symbols and parameters.

Symbol	Definition	Value	Unit
Fundamental constants and parameters			
m	Electron mass	510 999	eV/c2
c	Speed of light	299.792	nm/fs
$\hbar$	Planck's constant	0.658 212	ev fs
q	Unit charge	1	q
R_∞	Rydberg constant	13.605 7	eV
$\alpha_{\rm fs}$	Fine structure constant	1/137.036	⋯
ε_0	Permitivity of free space	$5.526\,35\times10^{-2}$	q^2/eV nm
Q	$\alpha_{\rm fs}\hbar c/4$	0.359 991	eV nm
F	Field at cathode	⋯	ev/nm
V	Potential	⋯	eV
Copperlike parameters			
μ	Chemical potential	7	eV
k_F	$(2m\mu)^{1/2}/\hbar$	13.554 6	1/nm
v_F	Fermi velocity	1.569 19	nm/fs
Φ	Work function	4.5	eV
FN field emission terms for Cu-like parameters			
A_o	$J_{\rm FN}$ parameter [Eq. (4)]	$3.138\,94\times10^{-5}$	A/eV^2
B	$J_{\rm FN}$ parameter [Eq. (4)]	65.207 3	eV/nm
κ	$J_{\rm FN}$ parameter [Eq. (4)]	0.772 81	⋯
$v(y)$	Elliptical integral function	$1-y^2\left[1-\frac{1}{3}\ln(y)\right]$	⋯
$t(y)$	Elliptical integral function	$\approx t(y_o)=1.061$	⋯
y_o	$e^{-1/2}$	0.606 531	⋯
PCM parameters			
r	PCM scaling parameter	⋯	⋯
n	PCM number of charges	⋯	⋯
a_0	Radius of emitter base	⋯	μm
$\rho_{\rm exp}$	dimensioned radial coordinate	⋯	nm
$z_{\rm exp}$	dimensioned axial coordinate	⋯	nm
l	tip-to-tip spacing	⋯	μm
L	Anode-cathode separation	⋯	nm, cm
a	dimensioned apex radius	⋯	nm
a_g	gete radius	⋯	μm
δ_t	time separation between emitted e^-	$q/I_{\rm tip}$	fs
$I_{\rm tip}$	current from one emitter	⋯	μA
$J(F_{\rm tip})$	current density at emitter apex	⋯	A/cm^2

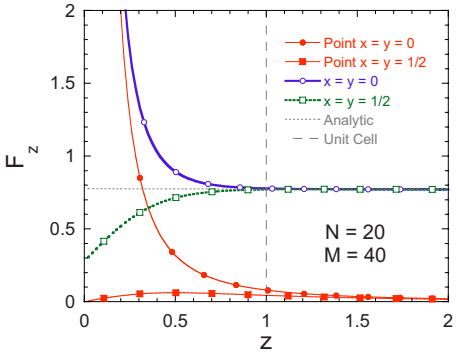

FIG. 1. (Color online) Behavior of the z component of field for a point charge and an array of point charges on ($x=y=0$) and off ($x=y=1/2$) the symmetry axis in units of tip-to-tip spacing. By $z=1$, the variations that exist in the field due to the discrete emission sites is largely (although not completely) diminished, suggesting $z=1$ to be the boundary between the unit cell region and the anode-cathode region.

Here, it is desirable to analytically obtain the field enhancement factor, the field variation over the apex of the emitter, and the potential variation on the axis of symmetry in a geometry that decouples the emitter apex shape from other features of the physical model (e.g., for a hyperbolic cone emitter, the cone angle is dependent on the anode-cathode separation[42]). Consequently, an analytical model of the emit-

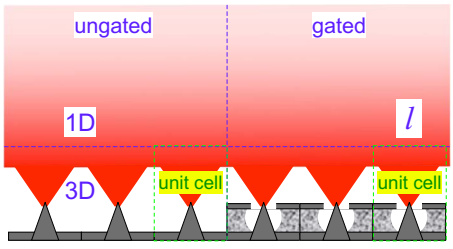

FIG. 2. (Color online) Schematic representation of the unit cell and 1D regimes suggested by Fig. 1 for gated and ungated geometries.

ter is developed that generalizes one used to study field emission and dark current in accelerators and referred to there as the PCM.[43]

The image charge FN equation

The FN equation, as widely used, is of a form traceable to Murphy and Good[44] and relies on elliptical integral functions $v(y)$ and $t(y)$. The best approximation to these functions has recently emerged[45,46] and leads to a different form of the FN equation than the most commonly used version in which $v(y)$ is assumed to be linear in y^2. Using the Forbes approximation to the elliptical integral function $v(y)$ and a representative constant for $t(y)$ (as in Table I), the general form of the FN equation is (albeit in a slightly different form than that given by Forbes[47])

$$J_{\mathrm{FN}}(F) = AF^{2-\kappa}\exp(-B/F), \tag{3}$$

where A, B, and κ are constant (or nearly so) and given by

$$\kappa = \frac{8Q}{9\hbar}\sqrt{\frac{2m}{\Phi}},$$

$$A = \frac{q}{16\pi^2\hbar\Phi t(y_o)^2}\left(\frac{\Phi^2 e^6}{4Q}\right)^{\kappa} \equiv A_o\left(\frac{\Phi^2 e^6}{4Q}\right)^{\kappa},$$

$$B = \frac{4}{3\hbar}\sqrt{2m\Phi^3}, \tag{4}$$

and where B is equivalent to B_{FN} in Eq. 40 of Ref. 48, $y_o = e^{-1/2} = 0.6065$, $t(y_o) = 1 + (1/6e) = 1.061$, and other notations follow Ref. 43 or are in Table I. The constant y_o is such that the tangent line to the Forbes approximation to $v(y)$ is linear in y^2 with a slope of -1, which provides a connection to the usual (metal) result in that if $\kappa = 0$, then the usual representation is recovered. For copperlike parameters it follows that $\kappa = 0.772\,81$. While Eq. (3) is not in a form resembling the FN equation as originally derived, it is a consequence of the forms used for $v(y)$ and $t(y)$.

As a final observation, as discussed (and advocated) by Forbes,[47] the form of Eq. (3) removes the privileged role of so-called FN coordinates in which $\ln(J/F^2)$ is plotted against $1/F$, and—by extension—the same with $\ln(I_{\mathrm{tip}}/V^2)$ with $1/V$. In point of fact, $\ln(J_{\mathrm{FN}})$ will appear linear as a function of $1/F$ for a variety of κ values. The pedigree of Millikan–Lauritsen plots, in which $\ln(J)$ versus $1/F$ is shown, is older than FN, easier to use, more robust in dealing with corrections and sources of voltage dependence, and therefore shall be how $I(V)$ data shall be represented here.

The numerical model for a single emitter

The PCM gives field enhancement and tip radii parameters in a computationally expedient manner. A line of charges is placed along the z axis above the $z=0$ plane in such a manner as to have the zero equipotential line approximate the shape of an emitter. The potential everywhere is related to the background field F_o (in practice, the field at the virtual anode in the unit cell) to the base dimensions of the emitter characterized by a length scale a_0 via

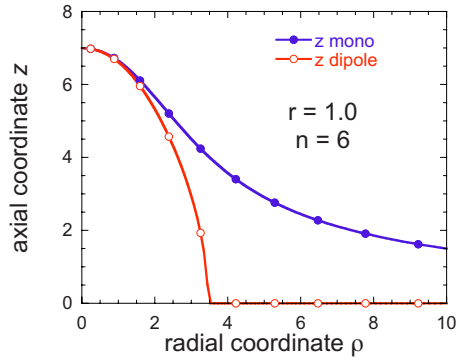

FIG. 3. (Color online) Comparison of the monopole versus dipole tips for $r=1$ and $n=6$.

$$V(\rho,z) \equiv F_o a_0 V_n\left(\frac{\rho_{\mathrm{exp}}}{a_0}, \frac{z_{\mathrm{exp}}}{a_0}\right),$$

$$V_n(\rho,z) \equiv -z + (\rho^2+z^2)^{-1/2} + \sum_{j=1}^{n}\frac{\lambda_j}{[\rho^2+(z-z_j)^2]^{1/2}}, \tag{5}$$

where λ_0 is implicitly set equal to 1 and, in the second line, ρ and z are dimensionless cylindrical coordinates and correspond to the ratio of the physical radial and axial coordinates with the unit a_0 such that $V_n(\rho,z)$ itself is dimensionless. The z_j are defined according to

$$z_n = \sum_{j=1}^{n-1} r^{n-1} = \frac{1-r^n}{1-r} \equiv S_n(r) \tag{6}$$

and denote the location of the nth charge of relative magnitude λ_n. The physical height of an n-charge emitter is $S_{n+1}(r)a_0$. The factor r is a scaling parameter such that a charge λ_j is placed r^j above the one below it (i.e., $z_{j+1} = r^j + z_j$). The values of λ_j are dictated by the boundary condition $V_n(0, z_{n+1}) = 0$, and the surface is defined by the zero equipotential line. Because charges of only one sign are considered in Eq. (5), V_n in Eq. (5) shall be termed the "monopole" model $V_n^{\mathrm{mono}}(\rho,z)$ to distinguish it from another version below. The monopole emitters have broad bases suitable to model cone formation from heating and melting. In contrast, microfabricated field emitters tend to be of a sharper conical shape and carbon nanotubes more cylindrical.[49] It is therefore useful to introduce a model that more closely approximates narrow geometries and called the "dipole" model $V_n^{\mathrm{dipl}}(\rho,z)$ because it considers pairs of opposite charges placed symmetrically about the z plane. The dipole V_n is defined by

$$V_n^{\mathrm{dipl}}(\rho,z) \equiv -z + \sum_{j=1}^{n}\lambda_j\{[\rho^2+(z-z_j)^2]^{-1/2} - [\rho^2+(z+z_j)^2]^{-1/2}\}, \tag{7}$$

where λ_0 is implicitly set equal to 0. It is subject to the same boundary condition $V_n^{\mathrm{dipl}}(0, z_{n+1}) = 0$. The presence of mirror image charges across the $z=0$ plane results in a much sharper, more ellipsoidal emitter shape, as shown in Fig. 3 for the particular case of $r=1$ and $n=6$. In both the monopole

and dipole models, the field enhancement factor β_n and apex radius a_n are given by

$$\beta_n(r) = -\partial_z V_n(0,z)\big|_{z=z_{n+1}},$$

$$a_n(r) = -\frac{\partial_\rho V_n(\rho,z)}{\partial_\rho^2 V_n(\rho,z)}\bigg|_{\rho=0,z=z_{n+1}}. \tag{8}$$

It is observed that Eq. (8) refers to *apex* values of field enhancement and radius, but Eq. (7) does not preclude the evaluation of such quantities off-axis (rather, the on-axis values are the most appropriate metric to discuss). The field and, hence, local field enhancement are readily evaluated from Eq. (7) off axis and down the sides of the emitter. Importantly, the PCM formulation allows for the treatment of small asymmetric protrusions existing on a conical emitter through the addition of an off-axis point charge in a straightforward manner or alternately a whisker that is bent and therefore no longer rotationally symmetric. These generalizations are useful extensions of the theory, but are not presently considered.

The methods to evaluate λ_n, β_n, and a_n in terms of r and n are now given. As may be anticipated, $\lambda_n(r)$ for small r is an exponentially shrinking quantity as n increases, and it is computationally expedient to introduce an auxiliary function $P_n(r)$ defined by

$$\lambda_n(r) \equiv P_n(r) r^n \tag{9}$$

to separate out the exponentially small behavior. The boundary conditions can now be concisely expressed by Eq. (5) and (7) evaluated at $\rho=0$ and $z=z_{n+1}$ via

$$\sum_{j=1}^{n} M_{n,j}^{\text{mono}}(r) P_j(r) = S_{n+1}(r) - \frac{1}{S_{n+1}(r)},$$

$$\sum_{j=1}^{n} M_{n,j}^{\text{dipl}}(r) P_j(r) = S_{n+1}(r). \tag{10}$$

In matrix parlance,

$$[\mathbf{M}^{\text{mono}}]_{n,j} = \frac{\theta_{n,j}}{S_{n+1-j}(r)},$$

$$[\mathbf{M}^{\text{dipl}}]_{n,j} = \frac{2S_j(r)}{S_{n+1-j}(r)[S_j(r)+S_{n+1}(r)]}\theta_{n,j}, \tag{11}$$

where $\theta_{n,j}=1$ if $j \leqslant n$ and 0 otherwise, and use has been made of $S_{n+1}-S_j = r^j S_{n+1-j}$. Equation (10) is therefore concisely expressed as matrix equation $\mathbf{M}\cdot\mathbf{P}=\mathbf{S}$, where $\mathbf{M}$ is a lower triangular matrix, and therefore the inversion $\mathbf{P}=\mathbf{M}^{-1}\cdot\mathbf{S}$ is easily accomplished using standard numerical techniques. Because $\mathbf{M}$ is lower triangular, the solution for $n=N$, where N is larger than any n likely encountered in practice (e.g., at $N=24$ and $r=0.4$, the base of a nanometer-radius emitter would be approximately 2 m), need be performed but once for a given r and the coefficients can be stored and therefore available for any $n<N$ in subsequent calculations. Such would be useful, for example, to model the physical growth of an emitter as n increases.

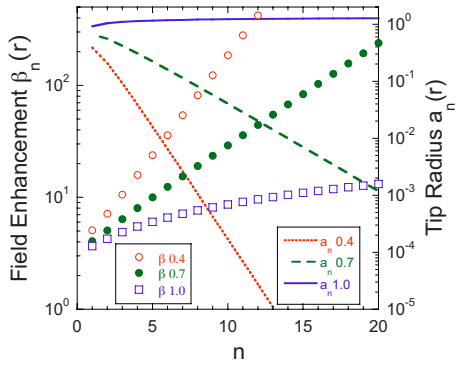

FIG. 4. (Color online) Dimensionless field enhancement factor β_n and apex radius factor a_n as a function of n using the dipole model of Eqs. (13) and (15). The numbers following β and a_n in the legend are the value of r for that line.

The matrix method can likewise be used to calculate the field enhancement factors $\beta_n(r)$, which like $P_n(r)$ can be cast as the solution to matrix equations. Define $\mathbf{B}$ by

$$[\mathbf{B}^{\text{mono}}]_{n,j} = \frac{1}{r^j (S_{n+1-j})^2},$$

$$[\mathbf{B}^{\text{dipl}}]_{n,j} = \frac{4S_j S_{n+1}}{r^j [S_{n+1-j}(S_{n+1}+S_j)]^2}, \tag{12}$$

where the argument in S_j is suppressed. Then

$$\beta^{\text{mono}} = \mathbf{B}^{\text{mono}}\cdot\mathbf{P} + \mathbf{Y},$$

$$\beta^{\text{dipl}} = \mathbf{B}^{\text{dipl}}\cdot\mathbf{P} + \mathbf{I}, \tag{13}$$

where $\mathbf{I}$ is the identity matrix and $[\mathbf{Y}]_n = 1+[S_n(r)]^{-2}$. As with $\mathbf{M}$, $\mathbf{B}$ is a lower triangular matrix and so all the field enhancement values for any $n \leqslant N$ can be obtained by inverting the matrix equation for $n=N$. The equations for apex radius can be put in the same form, but it is convenient to simply give them as, for the monopole case (the r dependence of the S terms is suppressed for visual clarity),

$$a_n^{\text{mono}} = S_{n+1}\frac{1 + S_{n+1}^2 + \sum_{j=1}^{n} \frac{P_j}{r^j}\left(\frac{S_{n+1}}{S_{n+1-j}}\right)^2}{S_{n+1}^3 + \sum_{j=1}^{n} \frac{P_j}{r^{2j}}\left(\frac{S_{n+1}}{S_{n+1-j}}\right)^3}, \tag{14}$$

and for the dipole case

$$a_n^{\text{dipl}} = 2\frac{\sum_{j=1}^{n} \frac{P_j}{r^j}\frac{S_j S_{n+1}}{[S_{n+1-j}(S_j+S_{n+1})]^2}}{\sum_{j=1}^{n} \frac{P_j}{r^{2j}}\frac{S_j(S_j^2+3S_{n+1}^2)}{[S_{n+1-j}(S_j+S_{n+1})]^2}}. \tag{15}$$

The behavior of the field enhancement factor and the apex radius for various r and n is shown in Fig. 4. To relate to physical emitters, the overall shape of the emitter is governed by type (cusplike corresponds to "mono," conical, or ellipsoidal to "dipl"), height is governed by $S_n(r)a_0^{\text{exp}}$, and apex radius is governed by $a_n(r)a_0^{\text{exp}}$, where a_0^{exp} is a dimensioned unit. In contrast to all other analytical emitter models,

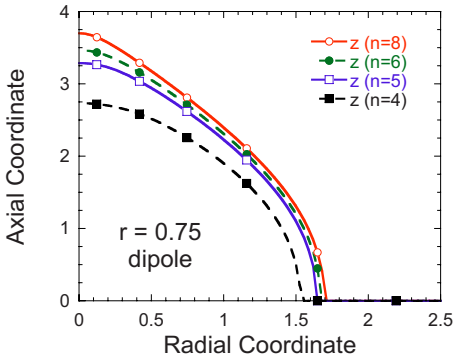

FIG. 5. (Color online) A dipole tip for $r=0.75$ and increasing values of n, demonstrating how the shape of the tip stays approximately the same even as the apex becomes sharper for increasing n.

the model retains the same basic emitter shape as the tip is progressively sharpened. This is seen in Fig. 5 as n increases for a given r.

The tip current model

Near the apex of the emitter, the surface is, to a good approximation, parabolic and therefore defined by the equation

$$z_{\mathrm{surf}}(\rho) \approx z_{n+1} - \frac{\rho^2}{2a_n}. \tag{16}$$

The current density drops rapidly as ρ increases because to a good approximation $F \approx F_{\mathrm{tip}} \cos\theta = F_{\mathrm{tip}}[1-(\rho/a_n)^2]^{1/2}$, where the cylindrical coordinate ρ is related to the spherical coordinate θ by $\rho = a_n \sin\theta$. For example, when ρ is 75% of a_n, then the current density is 1% of its apex, or "tip," value. The total current is obtained from[38]

$$I(F_{\mathrm{tip}}) = \int_\Omega J d\Omega = \int_0^\infty 2\pi\rho\sqrt{1+(\partial_\rho z_{\mathrm{surf}})^2}J[F(\rho)]d\rho$$
$$\approx 2\pi(a_0^{\mathrm{exp}}a_n)^2 J(F_{\mathrm{tip}})\int_0^1 x\sqrt{1+x^2}J[F(a_n x)]dx. \tag{17}$$

Using Eq. (16) in Eq. (3) gives

$$I(F_{\mathrm{tip}}) \approx \frac{1}{2}\pi a^2\left(\frac{\pi}{s}\right)^{1/2}\{\mathrm{Erf}[p(F)s(F)] - \mathrm{Erf}[s(F)]\}\exp(s(F)^2)J(F_{\mathrm{tip}}),$$

$$p(x) = \frac{5B-4(2-\kappa)x}{2B-2(1-\kappa)x},$$

$$s(x) = \frac{B-(1-\kappa)x}{\sqrt{2x[3B-2(3-\kappa)x]}}, \tag{18}$$

where $\mathrm{Erf}(x)$ is the error function and the tip radius is $a \equiv a_n a_0^{\mathrm{exp}}$ (and is therefore dimensioned). For example, an apex field of 8 GV/m, a tip radius of $a_0^{\mathrm{exp}}=10$ nm, and copperlike parameters, for which p and s are equal to 2.0945 and 3.6134, respectively, Eq. (17) predicts that $I_{\mathrm{tip}}=49.7$ μA, whereas Eq. (18) gives 52.7 μA. The notional emission area

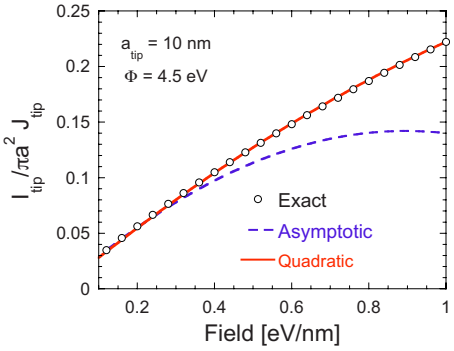

FIG. 6. (Color online) The notional emission area g factor [ratio of tip current I_{tip} to the product of the current density on axis with the area of a hemisphere of radius equal to the apex radius $\pi a^2 J(F_{\mathrm{tip}})$] calculated exactly (open circles), approximately using Eq. (19) (dashed line), and by the quadratic fit of Eq. (20) (solid line).

$(I_{\mathrm{tip}}/J_{\mathrm{tip}})$ is $0.176\,44\pi a^2$ corresponding to 55.431 nm^2. The field dependence of the notional emission area is shown in Fig. 6. Using the $r=0.4$ line of Fig. 4, this would be achieved by an emitter characterized by $a_0^{\mathrm{exp}}=1.5345$ μm and $n=6$ in a background field of 222.61 MV/m. For comparison, such a field is: a fraction of the breakdown fields associated with various metals; less than the 400 MV/m surface field that characteristic of the compact linear collider[50] and comparable to the ratio of the gate potential (75 V) to the gate radius (0.375 μm) for a Spindt-type field emitter operating at 50 mA for a 10^4 tip array.[27] Continuing, the dimensionless axis potential $V_n(0,z)$ and its gradient for $z \geqslant z_{n+1}$ are shown in Fig. 7 (albeit for $n=4$ rather than 6 to bring out the near-apex behavior) for a dipole geometry: by $z-z_{n+1} \approx 1$ (a distance characteristic of the emitter base radius) the field gradient is only 28% larger than the background field whereas the field enhancement factor is 15.855.

The coefficient of J in Eq. (18), or rather $g(F) \equiv I_{\mathrm{tip}}/(\pi a^2 J)$, is to a good approximation a quadratic function of F, albeit that its evaluation is somewhat cumbersome. It might be thought that a useful approximation can be obtained by using asymptotic expansions of the error function $\mathrm{Erf}(x) \approx 1-\pi^{-1/2}e^{-x^2}(x^{-1}-2x^{-3})$ to give

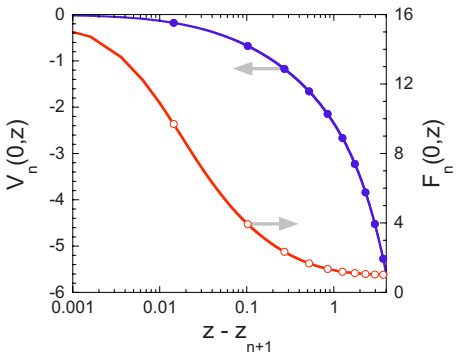

FIG. 7. (Color online) The dimensionless factor $V_n(\rho,z)$ of Eq. (7) (open circles) evaluated on axis ($\rho=0$) and its gradient (solid circles) with respect to z. The gradient is within 28% of its asymptotic value by $z=1$, indicating that field enhancement is curtailed at a length scale on the order of the emitter size.

$$g(F) \approx \frac{F(2 - s(F)^{-2})}{B + (1 - \kappa)F}, \tag{19}$$

but this approximation is poor when F approaches 10 eV/nm, as shown in Fig. 6. For computational purposes, it is better to exploit the quadratic behavior explicitly and take advantage of $g(0)=0$ to obtain

$$g(F) \approx F(c_1 F + c_0),$$

$$c_1 = 2g(F_{\max}) - 4g\left(\frac{F_{\max}}{2}\right),$$

$$c_0 = -g(F_{\max}) + 4g\left(\frac{F_{\max}}{2}\right), \tag{20}$$

where $F_{\max}=10$ eV/nm. For copperlike parameters, $c_1 = -0.064\,203$ and $c_2 = 0.286\,47$ and gives the line labeled "Quadratic" in Fig. 6, entailing that $g(F)$ therefore need only be computed twice for a good parametric representation.

The space charge model

With an estimate of I_{tip}, an evaluation of when space charge forces affecting emission for a single tip can be made. Assume that electrons are emitted along the z axis every $\delta t = q/I_{\text{tip}}$ with (in contrast to a previous treatment[36]) an initial velocity $v \equiv \hbar\langle k\rangle/m \approx \hbar k_F/m \equiv v_F$, where $\hbar^2 k_F^2/2m = \mu$.[16] Assume that the field that accelerates the emitted electron is constant. In actuality, the field drops away from the emitter apex as a consequence of geometry and so electrons will not be swept away as quickly as assumed. The effect of electrons further out (where the approximation degenerates) is much less than those closer to the emission site (where the approximation is good) because their influence fades as the square of their distance. Therefore, the cumulative space charge effect will be larger than that predicted by the constant field approximation which tends to underestimate it (i.e., the constant field result is a lower bound estimate). The distance of the jth electron from the apex is then

$$z_j(\delta t) = \frac{\hbar k_F}{m}(j\delta t) + \frac{F}{2m}(j\delta t)^2. \tag{21}$$

The sum of the forces on the apex of the emitter from the emitted electrons is

$$\delta F_e \approx \frac{q^2}{4\pi\varepsilon_0}\sum_{j=1}^{\infty}[z_j(\delta t)]^{-2}. \tag{22}$$

Let the image charge be that of a sphere of radius a, for which

$$\delta F_i \approx \frac{q^2}{4\pi\varepsilon_0 a}\sum_{j=1}^{\infty}\frac{z_j(\delta t) + a}{[z_j(\delta t)]^2}. \tag{23}$$

Introducing the dimensionless term $\eta(F) = 2\hbar k_F/F\delta t$ then the total reduction in field at the apex of the emitter due to the line of emitted charge is the sum of Eqs. (22) and (23), or

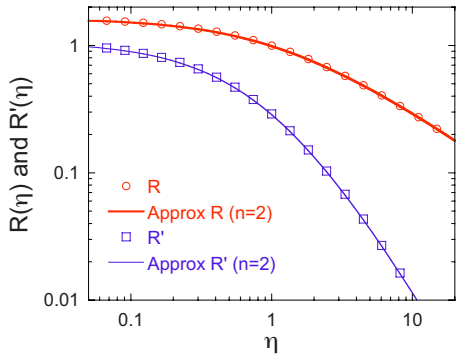

FIG. 8. (Color online) Behavior of R and R' [Eq. (25) with the approximations of Eqs. (26) and (27) for $n=2$].

$$\delta F = \delta F_e + \delta F_i \approx \frac{2a_{fs}\hbar cm}{aF\delta t^2}\left\{R(\eta) + \left(\frac{aF}{2\mu}\right)\eta^2 R'(\eta)\right\}. \tag{24}$$

The functions R and R' (where the prime does *not* indicate derivative) are defined by

$$R(x) = \sum_{j=1}^{\infty}\frac{1}{j(j+x)},$$

$$R'(x) = \sum_{j=1}^{\infty}\frac{1}{j^2(j+x)^2}. \tag{25}$$

Special cases are $R(0)=\zeta(2)=\pi^2/6$, and $R(1)=1$, and $R'(0) = \zeta(4) = \pi^4/90$ and $R'(1) = 2\zeta(2) - 3$, where $\zeta(n)$ is the Riemann zeta function. The summations can be approximated by equivalent integrals, but the error is largest for small j. Therefore, it is most efficient computationally to sum the first few terms and approximate the remainder by integration. We use

$$R(x) \approx \frac{1}{2n(n+x)} + \frac{1}{x}\ln\left(1 + \frac{x}{n}\right) + \sum_{j=1}^{n-1}\frac{1}{j(j+x)}. \tag{26}$$

For $n=2$, Eq. (26) is accurate to within 1.2%. Performing the same analysis with $R'(\eta)$ results in the approximation

$$R'(x) \approx \frac{2n(n+x)(2n+x) + x^2}{2n^2x^2(n+x)^2} - \frac{2}{x}\ln\left(1 + \frac{x}{n}\right) + \sum_{j=1}^{n-1}\frac{1}{j^2(j+x)^2}, \tag{27}$$

which for $n=2$ is accurate to within 0.6%. Larger n rapidly results in even greater accuracy. The behaviors of R and R' are shown in Fig. 8 for values of argument encountered for copperlike parameters (observe that n here is not the n of the PCM). The behavior of $\delta F(F)$ is shown in Fig. 9 for $a = 10$ nm and $\Phi = 4.5$ eV.

The field at the apex of the emitter is therefore smaller by δF than the field that would exist in the absence of space charge. The leading order estimate of single-tip space charge is then that the relationship between the field F at the apex to

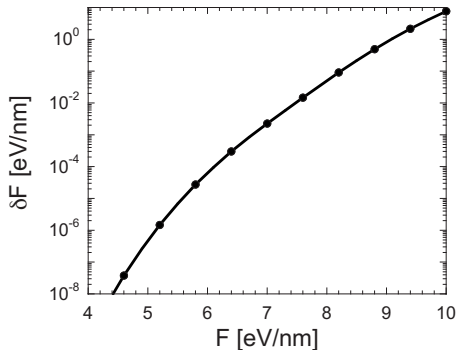

FIG. 9. Behavior of δF for a dipole geometry with $a=10$ nm, work function=4.5 eV, and calculated using Eqs. (24) with $\delta t = q/I_{\text{tip}}$.

the anode voltage must be $2\beta_n V/Nl = F + \delta F$. From Fig. 4, exponential approximations for the dipole geometry for $r=0.4$ are given by

$$\beta_n(r=0.4) \approx 3.125e^{0.4095n},$$

$$a_n(r=0.4) \approx 1.390e^{-0.9067n}. \quad (28)$$

The results of the space charge effects evaluation are shown in Fig. 10 for several values of n for a dipole configuration under the assumption that the work function is 4.5 eV and the base radius a_0 is 1 μm. The F_o used as a background field has conceptual difficulties when being related to a *gated* field emitter, as it will bear a nontrivial relationship to the gate voltage and gate radius, and requires modeling specifics beyond the present treatment (but intimated elsewhere[36]). The behavior shown in Fig. 10 for small large macroscopic field [given by $(F+\delta F)/\beta_n$] shows the impact of tip sharpening on the onset of space charge effects and bears a qualitative similarity to data shown in Ref. 27 and 36 (albeit the latter are shown on traditional FN plots): however, when emission is from an array, it is far more likely that space charge between the anode-gate planes causes the characteristic turnover than the single-tip effects of Fig. 10. To model further space charge effects on arrays, the 3D tip model must be embedded in the 1D gap model, and such an analysis shall be deferred to a separate study.

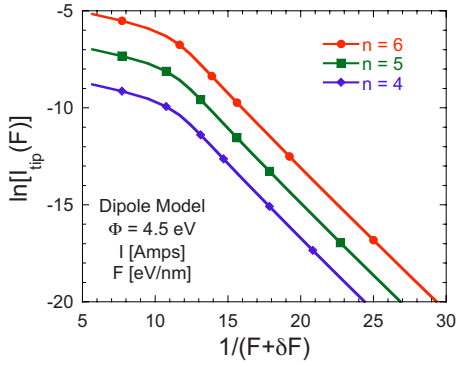

FIG. 10. (Color online) Tip current on a Millikan–Lauritsen plot evaluated using Eq. (18) (where increasing n refers to sharper emitters as per the PCM) and for a work function of 4.5 eV showing the effects of emitted charge on the FN behavior of a single (micro) emitter tip as a function of n for field enhancement and apex radius factors as given by Eq. (28). The units are amperes for current and eV/nm for field.

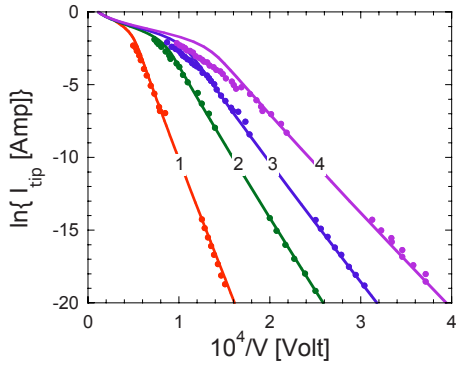

FIG. 11. (Color online) Comparison of the onset of space charge effects on the experimental data of Barbour *et al.* for a tungsten tip progressively covered with barium (1=no barium; 4=maximum coverage of barium) as shown on a Millikan–Lauritsen plot. Barium causes the work function to decrease, thereby changing the FN characteristics.

Comparison to experiment

Therefore, for comparison, consider a sharpened needle rather than a microtip, and, in particular, for field emission data from a tungsten emitter examined by Barbour *et al.* (Fig. 3 in Ref. 29) in which current intensified as barium was added to the needle to lower the work function. The experimental data allow for a comparison to the theoretical model after the specification of work function, tip radius, and field enhancement factor. First, the emission area of the needle is far larger than for the Spindt-type emitters: as a result, the reported apex radius of the emitter can be measured instead of inferred. Second, as the uncoated tip was tungsten, the field enhancement factor for the needle can be obtained from that tip and used for the coated tip measurements. Third, with the field enhancement factor and the apex radius, the work function for the remaining three lines corresponding to increased barium coverage of the tip can be determined. It needs to be emphasized that the *single* unknown quantity for each line (field enhancement factor for uncoated needle, work function for partially coated needle) can be found from a single I(V) data point using Eq. (18) rather than from least squares fitting to find slopes and intercepts on a FN plot.

The apex radius of the tungsten emitter is suggested by the measurements of Ref. 29 to be 364 nm. Using an I(V) data point extracted from line 1 (uncoated tungsten) from Fig. 3 of Ref. 29 ($V=7980.6$ V, $I=0.646$ μA), the field enhancement is determined to be $\beta=4516q$/cm. Using single data points from the other lines 2–4 at comparable current levels, and taking $v_F = c/152.4$ (the chemical potential of tungsten is greater than that of copper), the work functions of the partially coated tips are determined to be 3.30, 2.89, and 2.52 eV, respectively. I(V) data are then generated using Eqs. (18) and (24). The anode voltage is determined by $V=(F+\delta F)/\beta$, and the theoretical estimates of space charge affected emission from the tip are shown, along with the data of Barbour *et al.* in Fig. 11, where, following the recommendation of Forbes,[47] a Millikan–Lauritsen, rather than FN, coordinate plot is used: the numbering of the lines corresponds to the same numbering as used by Barbour *et al.* As noted previously, the assumption of a constant (versus a declining) field away from the emitter apex entails that the magnitude

of δF will be underestimated, but it is seen that even for unoptimized parameters, the prediction of the onset of space charge effects is quite clearly predicted.

CONCLUSION

Field emission is particularly subject to space charge effects because of the strong variation in the emitted current with the field that exists. Because of the high current densities that are possible with field emission, space charge effects can manifest themselves in two ways: first, it can suppress the macroscopic field between cathode and anode as would exist for an array of emitters (and as described by the usual Child's law formulation), and second, for a single emitter, charge near the emitter site can reduce the apex field. In the present work, a theory for the latter effect was developed and used to analyze single emitter data in the literature. It was determined that space charge can have an impact even for a single field emitter, and a method to estimate that impact was given. Finally, a discussion of the method to incorporate such a unit cell model into a larger macroscopic model, in a manner suggested to be useful to the needs of PIC codes, was given.

ACKNOWLEDGMENTS

We gratefully acknowledge support provided by the Naval Research Laboratory and the Joint Technology Office. We also thank A. Rokhlenko and J. L. Lebowitz (Rutgers University) and P. G. O'Shea and D. W. Feldman (University of Maryland) for helpful discussions.

[1]W. D. Jensen, F. B. Gerhard Jr., and D. M. Koffman, in *Van Nostrand's Scientific Encyclopedia*, edited by G. D. Considine and P. H. Kulik (Wiley, New York, 2005), p. 1771.
[2]P. Kruit, M. Bezuijen, and J. E. Barth, J. Appl. Phys. **99**, 024315 (2006).
[3]M. J. Fransen, M. H. F. Overwijk, and P. Kruit, Appl. Surf. Sci. **146**, 357 (1999).
[4]D. Morris, B. Gilchrist, and A. Gallimore, AIP Conf. Proc. **552**, 467 (2001).
[5]C. M. Marrese, J. E. Polk, K. L. Jensen, A. D. Gallimore, C. A. Spindt, R. L. Fink, and W. D. Palmer, in *Micropropulsion for Small Spacecraft*, edited by M. M. Micci and A. D. Ketsdever (American Institute of Aeronautics and Astronautics, Reston, VA, 2000), p. 18.
[6]V. L. Granatstein, R. K. Parker, and C. M. Armstrong, Proc. IEEE **87**, 702 (1999).
[7]R. K. Parker, R. H. AbramsJr., B. G. Danly, and B. Levush, IRE Trans. Microwave Theory Tech. **50**, 835 (2002).
[8]J. H. Booske, Phys. Plasmas **15**, 055502 (2008).
[9]J. W. Lewellen and C. A. Brau, Nucl. Instrum. Methods Phys. Res. A **507**, 323 (2003).
[10]J. W. Lewellen, in *Particle Accelerator Conference*, Proceedings of the IEEE Particle Acceleration Conference, 2005, p. 563.
[11]R. Ganter, R. J. Bakker, C. Gough, M. Paraliev, M. Pedrozzi, F. Le Pimpec, L. Rivkin, and A. Wrulich, Nucl. Instrum. Methods Phys. Res. A **565**, 423 (2006).
[12]C. H. Boulware, J. D. Jarvis, H. L. Andrews, and C. A. Brau, Int. J. Mod. Phys. A **22**, 3784 (2007).
[13]R. Ganter, R. Bakker, C. Gough, S. C. Leemann, M. Paraliev, M. Pedrozzi, P. Le Pimpec, F. V. Schlott, L. Rivkin, and A. Wrulich, Phys. Rev. Lett. **100**, 064801 (2008).
[14]M. Reiser, *Theory and Design of Charged Particle Beams* (Wiley, New York, 1994).
[15]A. Rokhlenko, K. L. Jensen, and J. L. Lebowitz, "Space charge effects in field emission: One dimensional theory", J. Appl. Phys. **107**, 014904 (2010).
[16]K. L. Jensen, P. G. O'Shea, D. W. Feldman, and J. L. Shaw, J. Appl. Phys. **107**, 014903 (2010).
[17]J. S. Fraser and R. L. Sheffield, IEEE J. Quantum Electron. **23**, 1489 (1987).
[18]D. H. Dowell, K. J. Davis, K. D. Friddell, E. L. Tyson, C. A. Lancaster, L. Milliman, R. E. Rodenburg, T. Aas, M. Bemes, S. Z. Bethel, P. E. Johnson, K. Murphy, C. Whelen, G. E. Busch, and D. K. Remelius, Appl. Phys. Lett. **63**, 2035 (1993).
[19]P. Michelato, Nucl. Instrum. Methods Phys. Res. A **393**, 455 (1997).
[20]R. A. Kishek, S. Bernal, C. L. Bohn, D. Grote, I. Haber, H. Li, P. G. O'Shea, M. Reiser, and M. Walter, Phys. Plasmas **10**, 2016 (2003).
[21]D. A. Dimitrov, D. I. Bruhwiler, J. R. Cary, P. Messmer, P. Stoltz, K. L. Jensen, D. W. Feldman, and P. G. O'Shea, in *Particle Accelerator Conference*, Proceedings of the IEEE Particle Acceleration Conference, 2005, p. 2583.
[22]J. J. Petillo, E. M. Nelson, J. F. Deford, N. J. Dionne, and B. Levush, IEEE Trans. Electron Devices **52**, 742 (2005).
[23]B. E. Carlsten, Nucl. Instrum. Methods Phys. Res. A **550**, 14 (2005).
[24]E. M. Nelson and J. J. Petillo, IEEE Trans. Plasma Sci. **32**, 1223 (2004).
[25]C. A. Spindt, I. Brodie, L. Humphrey, and E. R. Westerberg, J. Appl. Phys. **47**, 5248 (1976).
[26]P. R. Schwoebel and I. Brodie, J. Vac. Sci. Technol. B **13**, 1391 (1995).
[27]C. A. Spindt, I. Brodie, C. E. Holland, and P. R. Schwoebel, in *Vacuum Microelectronics*, edited by W. Zhu (Wiley, New York, 2001), p. 105.
[28]P. R. Schwoebel, C. A. Spindt, and C. Holland, J. Vac. Sci. Technol. B **23**, 691 (2005).
[29]J. P. Barbour, W. Dolan, J. Trolan, E. Martin, and W. Dyke, Phys. Rev. **92**, 45 (1953).
[30]R. G. Forbes, J. Vac. Sci. Technol. B **17**, 526 (1999).
[31]Y. Y. Lau, D. Chernin, D. G. Colombant, and P. T. Ho, Phys. Rev. Lett. **66**, 1446 (1991).
[32]D. Nicolaescu, J. Vac. Sci. Technol. B **11**, 392 (1993).
[33]Y. Y. Lau, Phys. Rev. Lett. **87**, 278301 (2001).
[34]R. Miller, Y. Y. Lau, and J. H. Booske, Appl. Phys. Lett. **91**, 074105 (2007).
[35]D. A. Kirkpatrick, A. Mankofsky, and K. T. Tsang, Appl. Phys. Lett. **60**, 2065 (1992).
[36]K. L. Jensen, M. Kodis, R. Murphy, and E. Zaidman, J. Appl. Phys. **82**, 845 (1997).
[37]J. D. Zuber, K. L. Jensen, and T. E. Sullivan, J. Appl. Phys. **91**, 9379 (2002).
[38]K. L. Jensen, in *Vacuum Microelectronics*, edited by W. Zhu (Wiley, New York, 2001), p. 33.
[39]R. L. Hartman, W. A. Mackie, and P. R. Davis, J. Vac. Sci. Technol. B **14**, 1952 (1996).
[40]K. L. Jensen, E. Zaidman, M. Kodis, B. Goplen, and D. Smithe, J. Vac. Sci. Technol. B **14**, 1942 (1996).
[41]Y. Feng and J. Verboncoeur, Phys. Plasmas **12**, 103301 (2005).
[42]K. L. Jensen, J. Vac. Sci. Technol. B **21**, 1528 (2003).
[43]K. L. Jensen, Y. Y. Lau, D. W. Feldman, and P. G. O'Shea, Phys. Rev. ST Accel. Beams **11**, 081001 (2008).
[44]E. L. Murphy and R. H. Good, Phys. Rev. **102**, 1464 (1956).
[45]R. G. Forbes, Appl. Phys. Lett. **89**, 113122 (2006).
[46]J. H. B.Deane and R. G. Forbes, J. Phys. A: Math. Theor. **41**, 395301 (2008).
[47]R. G. Forbes, J. Appl. Phys. **105**, 114313 (2009).
[48]K. L. Jensen, J. Appl. Phys. **102**, 024911 (2007).
[49]W. Zhu, *Vacuum Microelectronics* (Wiley, New York, 2001).
[50]M. Kildemo, S. Calatroni, and M. Taborelli, Phys. Rev. ST Accel. Beams **7**, 092003 (2004).